Journal of Sound and Vibration (1997) **203**(2), 341–351

LETTERS TO THE EDITOR

JOINT STIFFNESS CONTROL OF A ONE-LINK FLEXIBLE ARM

J. PUN† and S. E. SEMERCIGIL

Department of Mechanical Engineering, Victoria University of Technology, Footscray Campus, PO BOX 14428, MCMC, Melbourne, Victoria 8001, Australia

(*Received* 30 *May* 1995)

1. INTRODUCTION

The advantages of light and flexible arms over conventional rigid arms on robots include increased payload-to-weight ratio, quicker point-to-point movements, lower power consumption, smaller actuators and safer interactions with the environment. However, the use of light arms is severely limited by the lack of simple and effective vibration controllers to reduce end-point positioning and tracking inaccuracies caused by arm flexibility.

A simple method is presented here quickly to suppress impact-induced transient end-point vibrations (positioning errors) in a single-link flexible-arm using a semi-active joint controller. The method is based on the principle of variable stiffness control (VSC) and achieves the control by exploiting the potential energy storage capabilities of springs. Some research has already demonstrated the effectiveness of employing variable stiffness members to reduce unwanted vibrations, and can be found in references [1–3]. However, most applicable to this study is the work done by Warkentin and Semercigil [1], in which the effectiveness of VSC in suppressing the transient and random vibration of a single-link flexible arm was demonstrated. The flexible arm consisted of two identical beams (one active and one passive) mounted in a parallel configuration. Control was achieved by changing the boundary condition that in turn varied the bending stiffness of the controller beam, and thereby producing the desired control action. Unfortunately, the required special design possibly rendered the implementation of this stiffness controller impractical as an add-on controller for existing flexible arms.

The purpose of this work is to improve upon the work of reference [1] by using the joint stiffness of the base actuator rather than the bending stiffness of an additional beam. Hence, the controller is simplified significantly such that it can be implemented for a class of existing single-link flexible arms with minimal effort and little change to the structure of the arm.

1.1. *Variable stiffness control*

A brief description of VSC will be presented here for completeness. A more complete treatment may be found in references [1–3]. It is also recognized that although the single-link flexible arm to be controlled is a considerably more complicated structure, an undamped single-degree-of-freedom (SDOF) oscillator will be used to demonstrate the control method. Likewise, the similarities and differences between this simplistic SDOF model and more realistic systems will be discussed.

The undamped SDOF oscillator shown in Figure 1 has two possible stiffness values. The effective stiffness of the system is K when the clamp is applied, and $K - \Delta K$ when the clamp is released. The VSC technique is based on changing the effective stiffness of the system

† Present address: The School of Dentistry, University of Western Ontario, Canada.

0022–460X/97/220341 + 11 $25.00/0/sv950605

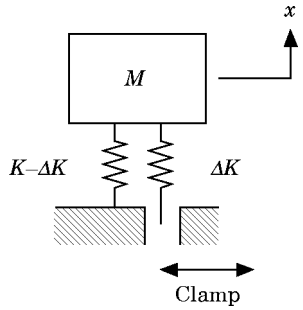

Figure 1. An undamped SDOF oscillator with VSC.

between these two states at peak displacement amplitudes. By very quickly unclamping and reclamping the active spring at instances of maximum displacements, potential energy is dissipated almost instantaneously (since the spring is assumed to have no inertia). Also, at the instant when the active spring is reclamped, a constant restoring force that opposes the velocity of oscillations (similar to a case of Coulomb friction) is imposed on the mass, since the equilibrium position of the active spring has shifted. It may be shown easily that the most effective stiffness ratio, $\kappa = \Delta K/K$, is 0·5, and would eliminate transient oscillations completely in just two actuations [1, 3]. Also, because VSC control is always dissipative, it is therefore unconditionally stable.

The single-link arm to be controlled is shown schematically in Figure 2. The arm will be described in detail in a subsequent section. The control action is implemented at the base by an actuator. The actuator is employed as the torsional active spring by manipulating its resisting torque to angular displacements at the joint. By using this technique, it is possible to release and recover the torque resistance of the actuator virtually instantaneously and thus implement the required control action. Hence, although the single-link arm is complicated considerably by the bending resilience of its links, the unconditional stability of the control will be maintained.

2. NUMERICAL SIMULATIONS

The single-link flexible arm investigated in this project is shown in Figure 2. The arm which consists of a flexible beam attached to a base actuator, models a flexible single-link robot with several simplifications. Located at the base are a pin-joint, two parallel torsional springs and a torsional viscous damper (not shown for clarity). The first torsional spring, $K - \Delta K$, represents the compliance (passive spring) of the joint, whereas the second torsional spring, ΔK, models the active spring of the controller. Finally, the torsional viscous damper approximates the frictional dissipation in the joint. A lumped mass is located at the tip of the link to model the payload, M. The system is analogous to the simplistic SDOF system shown in Figure 1, whereby the torsional springs in the flexible arm represent the translational springs in the SDOF model.

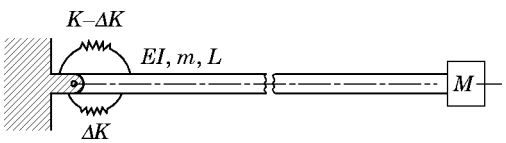

Figure 2. A model of a single-link flexible arm.

TABLE 1

Single-link flexible arm parameters used for simulation

Length, L	0·5 m
Mass/length, m	0·85 kg/m
Lumped tip mass, M	0·5 kg
Bending stiffness, EI	73 Nm^2
Passive elbow stiffness, $K - \Delta K$	100 Nm/rad
Active elbow stiffness, ΔK	100 Nm/rad
Elbow viscous damping coefficient	0·4 Nm/rad/s

The arm parameters used for the numerical simulation are shown in Table 1. These parameters are chosen to model a simple flexible system consisting of a thin 0·5 m long aluminum beam (of 50 mm × 6·25 mm rectangular cross-section) for its arm, and a 0·5 kg end-effector. The mass of the actuator is considered to be part of the base. A system with these parameters has a fundamental frequency of approximately 4·9 Hz and a payload-to-arm mass ratio of approximately 1·2. When compared with a conventional rigid-link robot, where a mass ratio of less than 0·1 is not uncommon [4], the 1·2 mass ratio of this arm is significantly larger.

Several assumptions are made before the system is modelled numerically: small oscillations are assumed to make linear analysis possible; the flexible arm is assumed to be a Euler–Bernoulli beam, ignoring shear deformations and rotary inertia; and, finally, the initial conditions are always assumed to be zero.

The results of the numerical simulation are produced by two FORTRAN programs. The first program uses the standard finite element method [5] to discretize the continuous system and produce global matrices. The second program uses the Newmark-β method [6] numerically to integrate the global matrices. Each integration time step is 0·005 s, which corresponds to approximately 1/41 of the fundamental oscillation period of the system. Generally, a 2 s simulation is found to provide sufficient time for the controlled cases to reach the settling time. The settling time is arbitrarily chosen, as a measure of the controller performance, and is assumed to be reached when the absolute tip displacement is less than 0·0001 m. The simulation is initiated by a half-sinusoid tip disturbance of $5 \sin(\omega_1 t)$ to simulate an impact of the arm with its environment. The fact that ω_1, the fundamental frequency of the system, varies with the parameters (such as an added mass on the arm) implies that the duration of the impact and ultimately the total energy input to the system also vary. This variable ω_1 ensures that the largest transient vibrations are produced for the uncontrolled cases. The variable stiffness control of the arm is accomplished by using the two torsional springs at the base joint, similar to the case discussed for the SDOF model in Figure 1.

3. NUMERICAL RESULTS

The numerical results in this section are presented to demonstrate the effectiveness and the versatility of the suggested controller for changing parameters of the arm. In addition, the effectiveness of a passive viscous damper at the base joint will be briefly investigated. The numerical simulations will be presented for varying the stiffness of the set spring ($K - \Delta K$), the viscous damping at the base, the payload (M) and the link length. Most of the results will be presented as surface plots, the horizontal axis (x-axis) of which represents time, the depth (y-axis) of which represents the parameter to be varied, and the vertical axis (z-axis) of which represents either the tip displacement or the base angle.

3.1. *The stiffness of the set spring*

The response of the uncontrolled case is determined for various stiffnesses of the passive spring. The purpose of these simulations is to decide a value of the stiffness that will maintain the integrity of the joint about its equilibrium position. The uncontrolled response of the base angle as the stiffness is increased from 20 to 400 Nm/rad is shown in Figure 3(a). As the stiffness increases, the flexibility decreases until the joint begins to lock up and produces a near-cantilever response. Moreover, as the stiffness increases, the fundamental frequency increases until it levels off when a cantilever response is exhibited. From these observations, a stiffness of 100 Nm/rad is chosen for each spring (the total stiffness is 200 Nm/rad) to provide some flexibility and to maintain joint integrity.

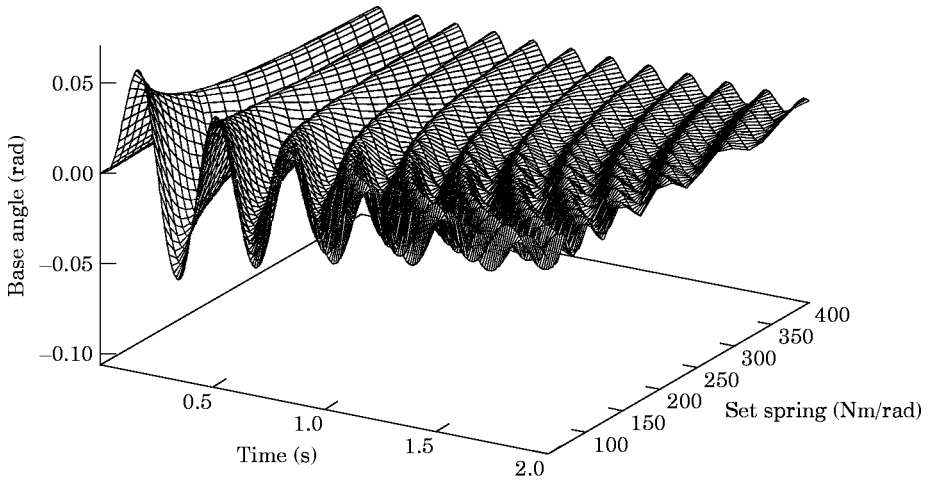

(a)

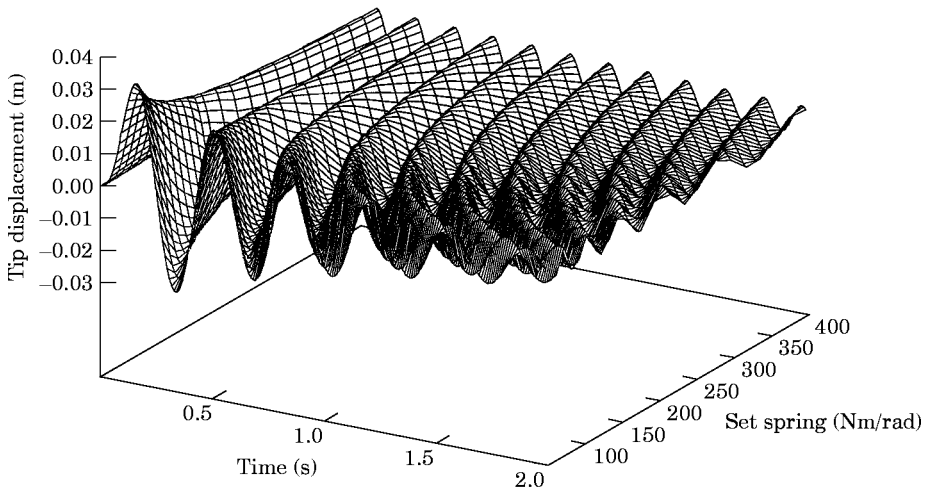

(b)

Figure 3. Histories of (a) the base angle and (b) the tip displacement for different set springs.

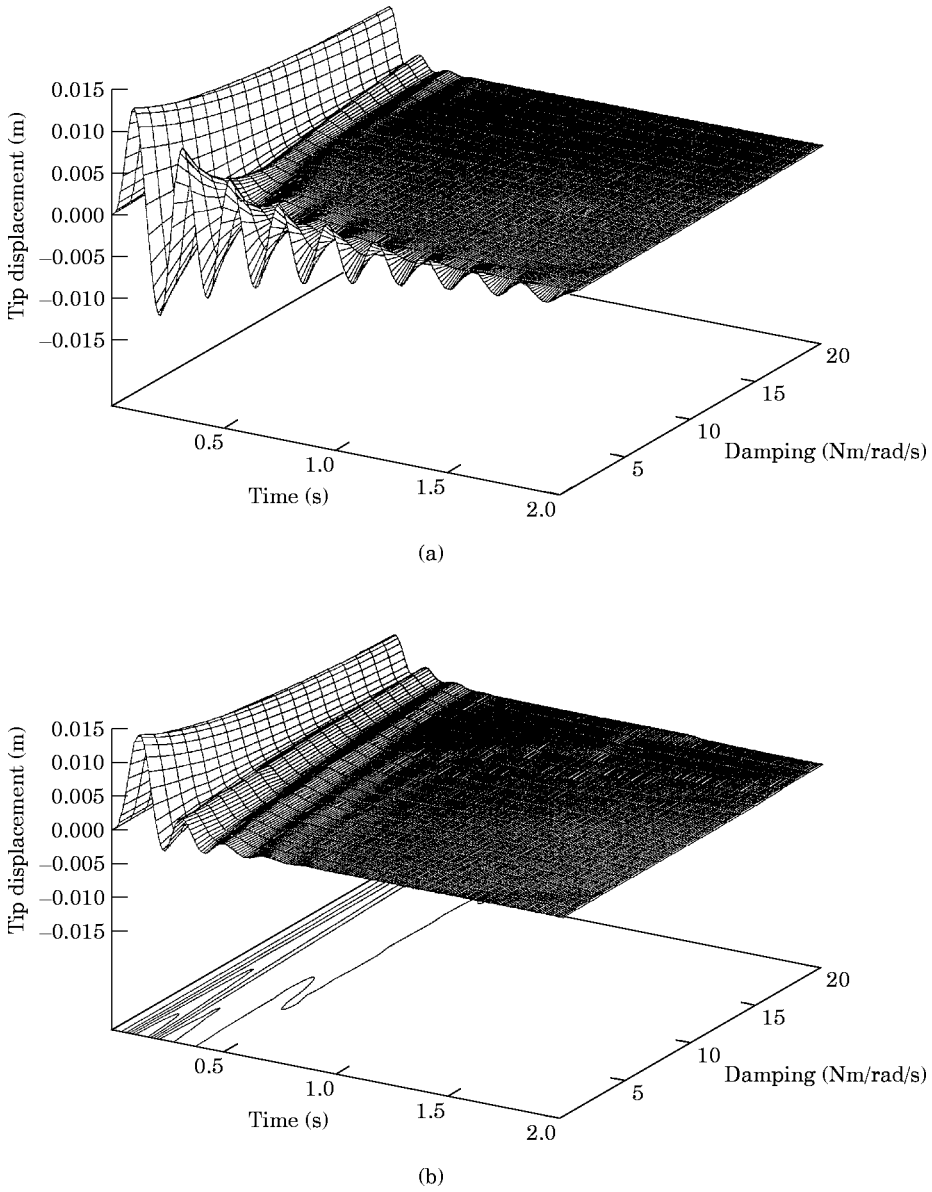

Figure 4. Histories of (a) the uncontrolled tip displacement and (b) the controlled tip displacement, showing the effect of damping.

Simulations in reference [1] suggest that equally matched passive and active springs produce the shortest settling times.

The correspondence between the vibrations at the base and at the tip is demonstrated in Figure 3(b). This figure is based on the same simulation parameters as in Figure 3(a), but here the tip response is shown. Comparisons between Figures 3(a) and (b) reveal that the trends observed in Figure 3(a) are almost identical to those in Figure 3(b). This is not surprising, considering that oscillations of the arm are expected to be primarily at the fundamental mode. Thus, subsequent simulations will show only the tip response, even though the system is assumed to have only a base sensor to implement the control action.

3.2. *A passive viscous damper*

In this section, a simple passive damper is investigated to determine its performance relative to that of the VSC. A light torsional viscous damper at the joint is normally used in the numerical model to approximate frictional dissipation at the joint. Hence, simulating the passive damper in this section simply involves increasing the damping parameter to larger values than required to approximate frictional losses in this section.

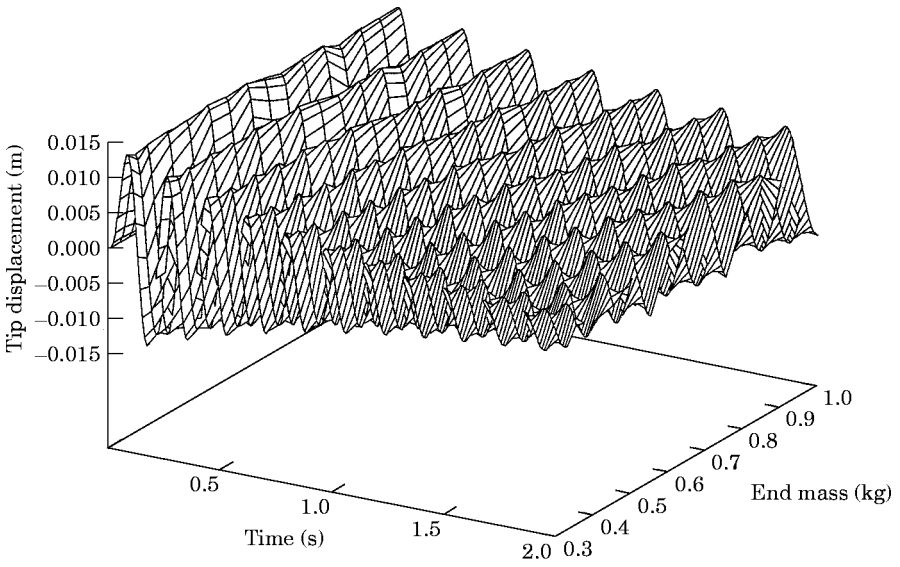

(a)

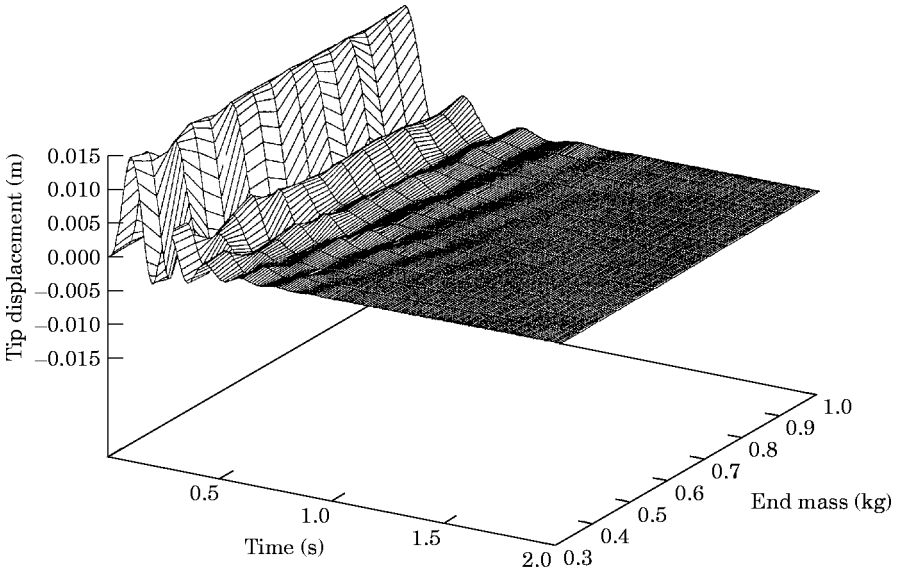

(b)

Figure 5. Histories of (a) the uncontrolled tip displacement and (b) the controlled tip displacement for different payload values, using a lightly damped joint.

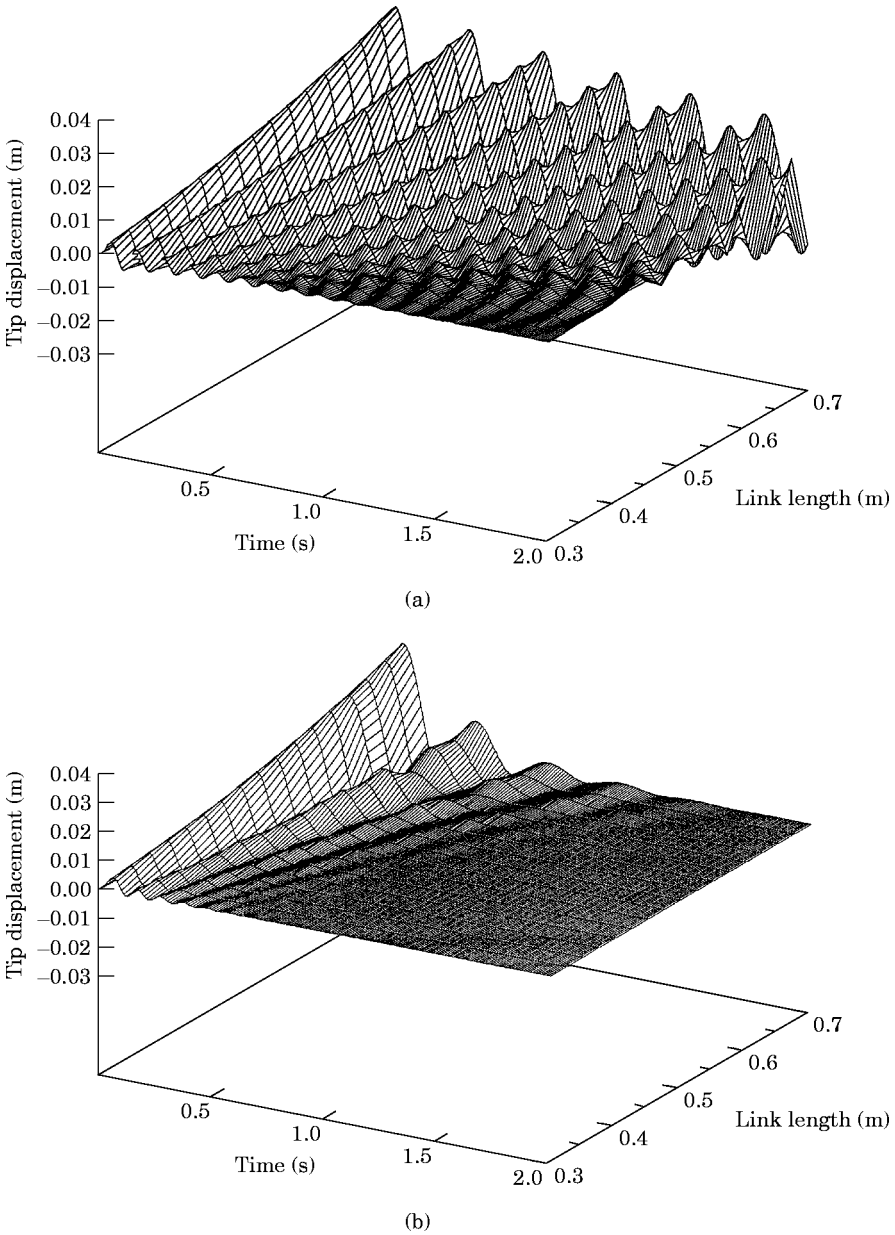

Figure 6. Histories of (a) the uncontrolled tip displacement and (b) the controlled tip displacement for different length values, using a lightly damped joint.

In Figure 4(a) is shown the uncontrolled response of the tip displacement as the torsional viscous damping coefficient at the joint is varied from 1 to 20 Nm/rad/s. The trend in this figure suggests that some moderate damping can be achieved with a damping value of 1 Nm/rad/s. The optimum passive damping is achieved with a value of approximately 10 Nm/rad/s. Beyond 10 Nm/rad/s, the base joint begins to gradually lock, as is apparent from the increasing amplitude of the second excursion. Simulations with viscous damping values beyond 20 Nm/rad/s do indeed demonstrate a joint lock-up and the resulting cantilever behaviour more clearly. The results in Figure 4(a) suggest that a viscous damper

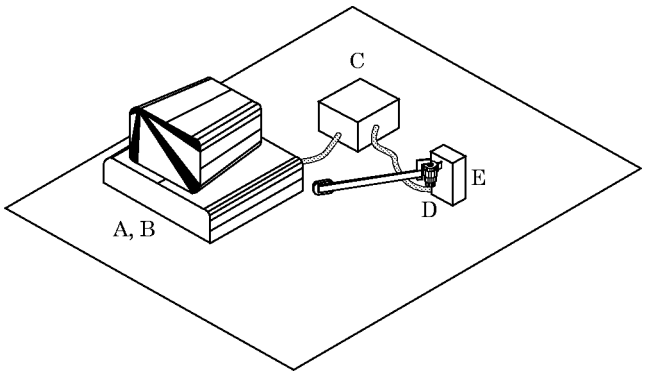

Figure 7. A rendering of the experimental set-up.

is able to control the transient oscillations of the single-link flexible arm described by the parameters in Table 1.

In Figure 4(b) is shown the controlled tip response of the same system as in Figure 4(a). With light viscous damping values, the VSC reduces the settling time considerably when compared with the same uncontrolled system. With larger damping values, relative improvement by VSC is not at all significant when compared with the uncontrolled case. This is mainly because little help is needed when there is sufficient viscous damping. However, it is important to note that VSC is always helpful, since it is always dissipative in nature.

It is clear from the comparisons between the uncontrolled and the controlled viscously damped cases that for the "given nominal parameters" of the arm, the passive damper is quite effective. However, because of its passive nature, its performance deteriorates as the arm parameters vary during operation [1–4]. These variations may include drastic changes in the payload mass (during pick-and-place operations), drastic changes in the arm length (as the reach of the arm needs to be varied), and drastic changes in the excitation parameters (unknown impact amplitude and duration). Hence, for the remainder of this study, minimal viscous damping will be considered at the base joint to model the frictional joint losses simply. Although it is recognized that frictional energy dissipation is different than that due to viscous damping, the practical advantage of the linear viscous model is its ease of implementation to the numerical simulation [1].

3.3. *Effect of payload with light damping*

A practical controller should be versatile enough to be effective even with large variations in payload, M. The uncontrolled response of the tip displacement as the tip mass is increased from 0·3 kg to 1 kg is shown in Figure 5(a). It is evident that as the tip mass

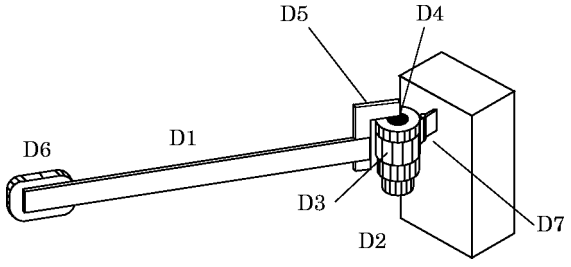

Figure 8. A close-up of the motor set-up.

TABLE 2

Single-link flexible arm parameters used for the experiment

Length, L	$0{\cdot}340 \pm 0{\cdot}001$ m
Mass/length, (m)	$0{\cdot}098 \pm 0{\cdot}002$ kg/m
Tip mass	$0{\cdot}054 \pm 0{\cdot}001$ kg
Bending stiffness, EI	$0{\cdot}37 \pm 0{\cdot}02$ Nm^2
Passive elbow stiffness	$0{\cdot}22 + 0{\cdot}02$ Nm/rad
Active elbow stiffness	$0{\cdot}27 \pm 0{\cdot}02$ Nm/rad
Equivalent elbow damping coefficient	0·004 Nm/rad/s

increases the fundamental frequency decreases and the system becomes somewhat more flexible. Consequently, the uncontrolled settling times take progressively longer to reach as payload mass increases. In Figure 5(b) is shown the controlled response for the same cases as in Figure 5(a). It is observed that even though the mass increases, the controlled settling time remains relatively constant at about 0·8 s. Again, it should also be realized that the energy transferred to the system by the impact varies with the payload, because the duration of the impact is always equal to half of the uncontrolled fundamental period of the system. This versatility gives VSC a significant advantage in an industrial environment.

3.4. *Effect of length with light damping*

The dynamic response of a flexible arm with a variable link length is simulated in this section. The purpose of this section is again to show the versatility of the VSC controller, this time for a range of length changes. The uncontrolled response as the link length is changed from 0·3 m to 0·7 m (about the nominal value of 0·5 m) is shown in Figure 6(a). It is evident that as the length increases, the fundamental frequency decreases and the system becomes more flexible. In Figure 6(b) is shown the corresponding controlled response of Figure 6(a). It is evident that VSC accomplishes the required control within 2 s for the entire range of link lengths.

4. EXPERIMENT

The accuracy of the numerical predictions is verified with a prototype of a single-link flexible arm. Figure 7 illustrates the basic set-up of the experiment, which includes a 386 personal computer (A), a DMC/400-10 PC-Servo Motion Controller (B) (located inside the computer), a Galil ICB/930 Interconnect Board (C), Pittman 19·1 V DC servo motor at the base of the arm (D) and a fixed wooden block (E) to which the base of the arm is clamped. The Interconnect Board provides a common connection point between the computer, the amplifier (on-board the Interconnect Board), and the servo motor.

As shown in Figure 8, the flexible arm, the parameters of which are listed in Table 2, consists of a flexible aluminium beam (D1) attached to a rigid mounting block (D2) via a servo motor (D3). The primary function of the servo motor is to serve as the active torsional spring to implement control at the base joint of the arm. The characteristic response of the motor could be programmed through its feedback system to allow the user to define the characteristics of the torsional spring. These characteristics are specified in reference [7]. The servo motor also has a built-in encoder with resolution of 2000 steps per revolution ($\pm 0{\cdot}0016$ rad). This encoder enables the servo motor to serve as the sensor to decide on the actuation instants and to record the history of the base angle. A passive torsional spring (D4) and a rigid aluminium bracket (D5) connect the base of the flexible

beam to the motor shaft. Payload mass (D6) is placed at the free end of the beam. A rigid brace (D7) attaches the servo motor on to the mounting block.

The experimental procedure consists of striking the tip of the flexible beam with a simple pendulum, which is released at a predetermined distance from the arm. The history of the base angle is then processed and actuation commands are generated as soon as a sign change of the slope of the base angle is detected. An actuation command results in releasing/recovering the torsional resistance of the servo motor to implement the control action. This simple excitation set-up provides a consistently repeatable transient disturbance. The signature of the transient disturbance is slightly skewed such that peak force is reached at about one-third of the contact duration. The history of transient force was recorded with a PCB-208B force transducer and a Kistler 5134 power supply/amplifier. This force was approximated with a half-sinusoid function, 14·6 sin(285t) N, in numerical simulations for comparison purposes between the predicted and measured resonse.

Typical histories of the uncontrolled base angle for both simulation (· · · ·) and experiment (—) are shown in Figure 9(a). Generally, the two sets of results agree quite closely up to approximately 10 s. After 10 s, the experimental model's response starts to decay faster than that of the numerical model, especially towards the end of the observation period. It may be speculated that this difference is due to the presence of frictional resistance at the joint which seem to stiffen as the amplitude of oscillation decays. It is not possible to capture this *hardening* behaviour with the present linear-model simulation.

The controlled response of the same case is shown in Figure 9(b). It is clear that there is close correspondence between the experiment and simulation. After the initial excitation, both models overshoot the equilibrium twice before settling. If the settling time is assumed to be the time at which the maximum amplitude is less than $\pm 0{\cdot}01$ rad, then the controlled experiment reaches it in 1·6 s while the controlled simulation reaches it in 1·5 s. Given that the settling time for the uncontrolled experiment is 13·2 s, the controlled case reaches settling time approximately 8·25 times faster than the uncontrolled case. In the simulations, the controlled case reaches the settling time approximately 14·5 times faster. However, this seemingly large discrepancy is due to the arbitrary choice of the settling time criterion. The

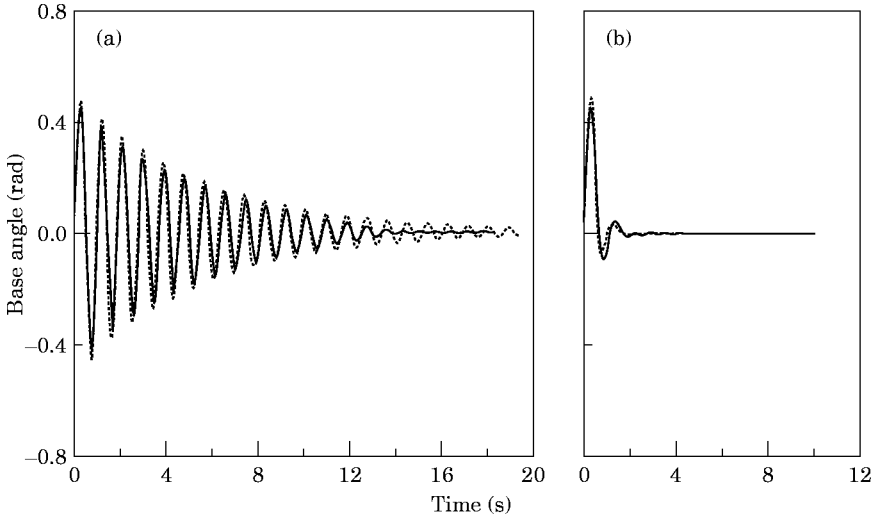

Figure 9. Histories of (a) uncontrolled base angle and (b) the controlled base angle for simulation (· · ·) and experiment (——).

agreement could be much closer for a different choice of settling time. Overall, the agreement between the experiments and the simulations is found to be quite acceptable.

5. CONCLUSIONS

A base controller using a variable stiffness technique has been presented for a single-link flexible arm with a compliant base joint. Overall, the prescribed control technique is versatile and relatively insensitive to large changes in arm parameters, such as payload and length change. The controller was shown only to take energy out of the system and was therefore unconditionally stable. The effectiveness of the controller was determined using computer simulations and a selected case was experimentally verified.

Implementing VSC on to a class of existing single-link flexible robotic arms is a simple task that requires only the addition of a servo motor and its supporting hardware. Additional sensors are not requried, since the encoder of the servo motor is sufficient for this purpose.

ACKNOWLEDGMENT

Financial support provided by the Natural Sciences and Engineering Research Council (NSERC) of Canada is acknowledged gratefully.

REFERENCES

1. A. Warkentin and S. E. Semercigil 1994 *Journal of Sound and Vibration* **187**, 1–21.. Variable stiffness control of a single link flexible robotic arm.
2. J. C. Chen 1984 *Journal of Spacecraft* **21**(5), 463–467. Response of large space structures with stiffness control.
3. J. Onoda, T. Endo, H. Tamaoki and N. Watanabe 1991 *American Institute of Aeronautics and Astronautics Journal* **29**(6), 977–983. Vibration suppression by variable-stiffness members.
4. B. Andeen (editor) 1988 *Robot Design Handbook*. New York: McGraw-Hill.
5. W. T. Thomson 1993 *Theory of Vibration with Applications*. Toronto: Prentice-Hall Canada; Fourth edition.
6. R. Craig JR 1981 *Structural Dynamics: an Introduction to Computer Methods*. Toronto: John Wiley.
7. J. Tal 1989 *Motion Control Applications*. Palo Alto, CA: Galil Motion Control.